Vermeer, P. A. (1990). *Géotechnique* **40**, No. 2, 223–236

The orientation of shear bands in biaxial tests

P. A. VERMEER*

Shear band formation in planar deformation of soil samples is studied theoretically to explain the experimental finding that orientation angles depend on particle sizes. A review of such data shows that steep Coulomb-type shear bands occur in fine sands, whereas less inclined Roscoe-type shear bands are observed for coarse material. A bifurcation analysis for the onset of shear-banding appears to be non-decisive, as all orientations within the Roscoe–Coulomb range are found to be admissible. The new element of this theoretical analysis is that the material outside the shear band is allowed to unload elastically. Hereafter the analysis is extended to the post-peak regime. Post-peak, the Coulomb-type shear band appears to be the weakest failure mode with the lowest residual strength. This explains the frequent occurrence of such shear bands. However, Coulomb-type shear bands are shown to involve stress discontinuities which can hardly occur in samples of coarse sand. This explains the occurrence of Roscoe-type shear bands as the latter do not involve stress discontinuities.

KEYWORDS: deformation; failure; friction; plasticity; shear tests.

La formation des bandes de cisaillement au cours de la déformation plane est examinée au point de vue théorique pour expliquer la découverte expérimentale que les angles d'orientation dépendent des grandeurs des particules. De telles données démontrent que des bandes raides de cisaillement type Coulomb se produisent dans les sables fins, tandis que des bandes de cisaillement moins inclinées type Roscoe sont obervées dans le cas des matieres grossières. Une analyse de bifurcation pour l'appariton des bandes de cisaillement paraît non-décisive, car toutes les orientations dans la gamme Roscoe–Coulomb se révèlent comme admissibles. Le nouvel élement dans cette analyse théorique est que la matière à l'extérieur de la bande de cisaillement se décharger élastiquement, consuite l'analyse est prolongée jusqu'au régime suivant le pic. Après le pic la bande de cisaillement paraît etre le mode le plus faible de rupture. Ceci explique l'apparition fréquente de telles bandes de cisaillement. On démontre cependant que les bandes de cisaillement type Coulomb impliquent des discontinuités de contrainte qui ne peuvent guère avoir lieu dans des échantillons de sable grossier. Ceci explique l'existence des bandes de cisaillement type Roscoe, puisque celles-ci ne comprennent aucunes discontinuites de contrainte.

INTRODUCTION

One of the most striking phenomena in soil bodies is the occurrence of shear bands, i.e. the localization of deformation in thin layers of intensively shearing material. For sand, a particular thickness of the band is visible; about 15 times the particle size. In a clay material, such a thickness is invisible and the shear band, or rupture layer, is viewed as a slip line.

In soil mechanics the phenomenon of shear banding was observed by Coulomb as early as 1776. He considered the orientation of a shear band against the direction of minor compressive stress (Fig. 1) to be

$$\theta_c = 45° + \phi/2 \qquad (1)$$

Discussion on this Paper closes 1 October 1990; for further details see p. ii.

* Delft University of Technology, The Netherlands.

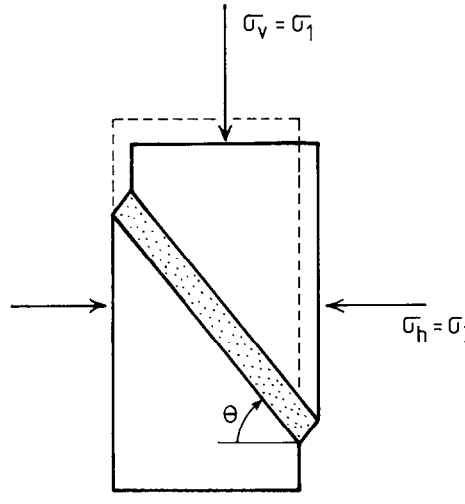

Fig. 1. Shear band in soil sample

where ϕ is the angle of internal friction. Such a shear band coincides with a plane of maximum stress obliquity. This concept was not disputed until 1970 when Roscoe presented the 10th Rankine lecture. Roscoe's solution for the shear band orientation stems from the use of a plastic flow rule, involving coaxiality for principal stress and plastic strain rate. It reads

$$\theta_R = 45° + \psi/2 \tag{2}$$

where ψ is the angle of dilatancy. For planar deformation this dilatancy angle (Roscoe, 1970) is defined as

$$\sin \psi = \frac{\dot{\varepsilon}_1^p + \dot{\varepsilon}_3^p}{\dot{\varepsilon}_3^p - \dot{\varepsilon}_1^p} \tag{3}$$

Here plastic strain rates are denoted by means of a superimposed dot. The superscript p is used to indicate plastic strains. The difference between the Coulomb orientation and the Roscoe orientation is quite significant, as the dilatancy angle is usually much smaller than the friction angle. The difference is of the order of 30°. Attempts to prove one or the other result, Equation (1) or Equation (2), have not been decisive as there is experimental evidence for both the Coulomb orientation and the Roscoe orientation.

The contents of this Paper are arranged as follows. In the next section experimental data are reviewed. The conclusion is that fine sand tends to yield Coulomb's shear band, whereas coarse sand tends to yield Roscoe-type bands. The observation that shear band orientations depend on particle sizes may seem inexplicable, but this is not the case as will be shown at the end of this paper.

In the third section the Mohr–Coulomb elasto-plastic model for soil behaviour will be described. In the fourth section this model will be used to simulate a simple shear test. The study of simple shear serves as an introduction to a proper shear band analysis, as shear banding is a localization of simple shear into narrow zones. The actual shear band analysis will consist of three parts.

First the onset of shear-banding (i.e. the bifurcation) is described analytically. Here the Paper will deviate from previously published analyses, as it will not be assumed *a priori* that the entire soil sample remains in a plastic state. Instead, the possibility of elastic unloading outside the shear band is accounted for. Various different shear band orientations are shown to be feasible.

Secondly, the post-bifurcation response of a biaxial sample is analysed numerically for a few different shear band orientations. Here the final residual strength is found to vary with the orientation of the shear band. Thirdly, a closed form solution is derived for the residual state of stress. The residual strength appears to reach a minimum for a particular orientation which is very close to the Coulomb-type shear band. Finally it is argued that this near-Coulomb orientation will occur in samples of fine sand rather than in coarse sand.

REVIEW OF THEORIES AND DATA

In 1977 Arthur, Dunstan, Al-Ani & Assadi renewed the debate on shear band orientations by reporting experimental evidence for an intermediate orientation of

$$\theta_A = 45° + (\phi + \psi)/4 \tag{4}$$

Later, Vardoulakis also published some such data. Moreover he presented theoretical backing for this intermediate orientation on the basis of a bifurcation analysis. Inspired by Vardoulakis's work the Author (1982) presented a simplified derivation for the above intermediate angle. However, it should be realized that the bifurcation analyses mentioned do not yield θ_A as the unique solution. It is found to be the shear band inclination for the lowest bifurcation point in the stress–strain curve, slightly before the full mobilization of the friction angle, as indicated in Fig. 2.

The importance of the bifurcation analyses mentioned is of a theoretical nature, as it had previously always been assumed that shear banding would only occur at peak stress or beyond the peak strength in the softening regime. At first the theoretical finding of pre-peak shear banding tempted researchers to jump to the conclusion that most, if not all, shear bands would emerge slightly before peak, but this is refuted by frequent observations of both Coulomb-type shear bands and Roscoe-type shear bands.

Rather than reviewing all existing data on shear band orientations, attention is restricted to data on the influence of the particle size. Data

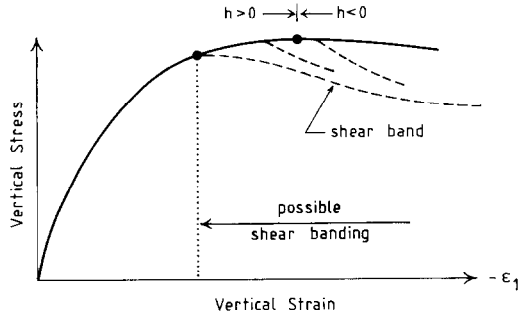

Fig. 2. Shear bands can start off at small rates of hardening or softening

obtained before 1982 are well reviewed by Arthur and Dunstan (1982), and they also added a great deal of new data. Their conclusions are as follows: rupture layers formed at failure in homogeneous stressed specimens with fixed principal stress directions are oriented at a specific angle, according to soil particle size between the limits of θ_R and θ_C. The rupture layer orientation changes with increasing soil particle size from the orientation of maximum stress obliquity (θ_C) towards no extension directions (θ_R).

Duthilleul (1983) measured shear band orientations in biaxial experiments on a Taylor–Schneebeli material; small bars made of PVC with diameters of 1·5 and 3 mm. The so-called 'particle' size of such a material is large, particularly with respect to the thickness of the surrounding rubber membrane. All his tests on many such samples of coarse material gave the Roscoe-type shear band with $\theta = \theta_R$, which is in line with Arthur's findings for coarse sand.

In 1984 Desrues reported results of about 20 biaxial tests on fine Hostun sand ($0{\cdot}125 < d < 0{\cdot}5$ mm). Shear band inclinations appear to be according to the Coulomb angle. The experiments were performed at the same laboratory as the ones by Duthilleul. Desrues (1984) tested fine Hostun sand at a cell pressure of 80 kPa both for a dense state and a loose state. For the dense sand, he observed shear band orientations in the narrow range between 65° and 69°, whereas the friction angle of 48° yields a Coulomb orientation of 69°. For the loose sand with a friction angle of 36°, and thus a Coulomb orientation of 63°, Desrues observed shear band orientations in the range between 57° and 64°.

Desrues' data show that fine sands yield shear band orientations that are just slightly below the Coulomb orientation. This is confirmed by most recent data by Desrues and Hammad (1989) for experiments with a wide range of cell pressures.

Vardoulakis (1988) also tested a fine sand to find the Coulomb solution. Hence Arthur's finding that Coulomb's solution applies to fine sands seems to be well established.

FROM HARDENING TO IDEAL PLASTICITY

At present complex constitutive soil models exist that involve effects of anisotropy and hysteresis in cyclic loading. For the present study an involved model is not needed, as a model within the framework of classical soil plasticity happens to be accurate at failure states where shear bands are formed. The general equation for an elasto-plastic model is

$$\dot{\boldsymbol{\varepsilon}} = \dot{\boldsymbol{\varepsilon}}^e + \dot{\boldsymbol{\varepsilon}}^p = \left[\mathbf{D}^{-1} + \frac{1}{h}\frac{\partial g}{\partial \boldsymbol{\sigma}}\frac{\partial f^T}{\partial \boldsymbol{\sigma}}\right]\dot{\boldsymbol{\sigma}} \tag{5}$$

where h is a hardening modulus, g is a plastic potential function, f is a yield function and

$$\boldsymbol{\varepsilon} = (\varepsilon_{xx}, \varepsilon_{yy}, \gamma_{xy})^T;\ \boldsymbol{\sigma} = (\sigma_{xx}, \sigma_{yy}, \sigma_{xy})^T \tag{6}$$

Plane strain situations are considered with $\dot{\varepsilon}_{zz} = 0$. The out-of-plane stress σ_{zz} is assumed to be the intermediate principal stress. The elasticity matrix is taken as simply as possible by defining

$$\mathbf{D} = \begin{bmatrix} 2G & 0 & 0 \\ 0 & 2G & 0 \\ 0 & 0 & G \end{bmatrix} \tag{7}$$

where G is the shear modulus. For convenience, Poisson's ratio is assumed to be zero. The attention is to be focused on soil behaviour near peak strength where elastic straining is of minor importance, so that there is no need for a sophisticated description of elastic effects. The inverse form of the elastoplastic relationship (5) reads

$$\dot{\boldsymbol{\sigma}} = \left[\mathbf{D} - \frac{1}{h+d}\mathbf{a}\mathbf{b}^T\right]\dot{\boldsymbol{\varepsilon}} \tag{8}$$

where

$$\mathbf{a} = \mathbf{D}\frac{\partial g}{\partial \boldsymbol{\sigma}} = G\left(2\frac{\partial g}{\partial \sigma_{xx}}, 2\frac{\partial g}{\partial \sigma_{yy}}, \frac{\partial g}{\partial \sigma_{xy}}\right)^T \tag{9a}$$

$$\mathbf{b} = \mathbf{D}\frac{\partial f}{\partial \boldsymbol{\sigma}} = G\left(2\frac{\partial f}{\partial \sigma_{xx}}, 2\frac{\partial f}{\partial \sigma_{yy}}, \frac{\partial f}{\partial \sigma_{xy}}\right)^T \tag{9b}$$

$$d = \frac{\partial f^T}{\partial \boldsymbol{\sigma}}\mathbf{D}\frac{\partial g}{\partial \boldsymbol{\sigma}} \tag{9c}$$

The hardening model given can be specified in more detail by means of a Coulomb-type yield function and a non-associated flow rule. Then this model can be used to explain shear-banding, as done by Mandel (1966), Vardoulakis (1980) and Vermeer (1982, 1984). Those analyses have shown that shear-banding is possible as soon as the hardening modulus h has decreased below a very small positive value slightly before peak strength (Fig. 2). As previous analyses have shown that shear-banding occurs for very small values of the hardening modulus, this parameter can now be neglected altogether. Indeed, h may be disregarded with respect to the much larger value of d, which is of the order of magnitude of the elastic shear modulus G. When h is neglected, Equation (8) becomes

$$\dot{\boldsymbol{\sigma}} = \mathbf{M}\dot{\boldsymbol{\varepsilon}} \qquad \mathbf{M} = \mathbf{D} - \frac{1}{d}\mathbf{a}\mathbf{b}^T \tag{10}$$

When this equation is used in shear band studies, it is obvious that the analysis will give no information on the question whether the shear band will occur slightly before or slightly beyond peak,

but one does expect to obtain information on the orientation of the bands.

The yield condition for $f = 0$ is now represented by a fixed failure surface in stress space. We have the so-called Mohr–Coulomb model by defining

$$\left.\begin{aligned} f &= \tau^* + \tfrac{1}{2}(\sigma_{xx} + \sigma_{yy}) \sin \phi - c \cos \phi \\ g &= \tau^* + \tfrac{1}{2}(\sigma_{xx} + \sigma_{yy}) \sin \psi \end{aligned}\right\} \quad (11)$$

where τ^* is the radius of Mohr's stress circle, namely

$$\tau^* = \sqrt{(\tfrac{1}{4}(\sigma_{xx} - \sigma_{yy})^2 + \sigma_{xy}^2)} \quad (12)$$

ϕ is the effective angle of internal friction and c is the effective cohesion. Similarly, all stresses are effective stresses and tension is taken as positive. With the given definitions of the yield function and the plastic potential, expressions for the vectors **a** and **b** in Equation (10) can be derived. Using Equations (9) it is found that

$$\mathbf{a} = G\begin{bmatrix} \cos 2\theta + \sin \psi \\ -\cos 2\theta + \sin \psi \\ \sin 2\theta \end{bmatrix}$$

$$\mathbf{b} = G\begin{bmatrix} \cos 2\theta + \sin \phi \\ -\cos 2\theta + \sin \phi \\ \sin 2\theta \end{bmatrix} \quad (13)$$

$$d = G(1 + \sin \psi \sin \phi) \quad (14)$$

with

$$\cos 2\theta = (\sigma_{xx} - \sigma_{yy})/2\tau^*$$

$$\sin 2\theta = \sigma_{xy}/\tau^* \quad (15)$$

The angle θ has a clear physical meaning; it is the angle between the x-axis and the minor compressive stress as shown in Fig. 3. This definition of θ may seem to differ from the use of θ as a shear band orientation, but the matter is harmonized by choosing the x-axis in the direction of the shear band as indicated in Fig. 5.

SIMULATION OF SIMPLE SHEAR

In this section a simple shear test is considered in order to obtain insight into the performance of the elastoplastic model and the shear-band mechanism. Although deformations tend to be heterogeneous in simple shear devices (Wood & Budhu, 1980), the sample is assumed to deform uniformly as indicated in the inset to Fig. 4a. Consider a dense cohesionless sand with the following properties.

$$G = 10\,\text{MPa} \quad \phi = 40^\circ \quad \psi = 10^\circ \quad c = 0$$

Two different initial stress states will be considered; a normally consolidated sample with initial state A and a heavily overconsolidated sample with initial state B.

sample A: $\sigma_{xx} = -25\,\text{kPa}$

$\sigma_{yy} = -100\,\text{kPa}$

$\sigma_{xy} = 0$

sample B: $\sigma_{xx} = -400\,\text{kPa}$

$\sigma_{yy} = -100\,\text{kPa}$

$\sigma_{xy} = 0$

In general, normally consolidated sand will show K_0 values above the ratio of 25/100, but an extreme situation is considered here. Similarly, the effect of overconsolidation is exaggerated by adopting $K_0 = 400/100$.

Equation (10) is used to compute the evolution of the stresses during the tests. For a simple perfect plasticity model as given by Equation (10), each stress–strain curve begins with an elastic range. The elastic response is linear with no change of σ_{xx} and σ_{yy} whereas σ_{xy} increases along with γ_{xy} according to $\sigma_{xy} = G * \gamma_{xy}$. The fully elastic response continues until the yield condition $f = 0$ is satisfied.

The normally consolidated sample shows a small elastic range up to a shear stress of about 15 kPa (Fig. 4a), but the overconsolidated sample behaves elastically up to a shear stress of nearly 60 kPa. As soon as the yield condition is satisfied

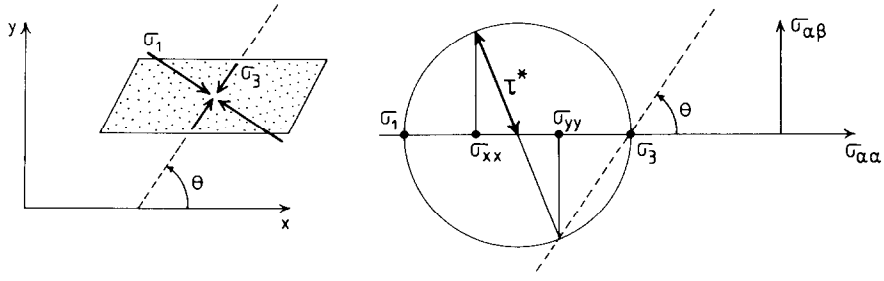

Fig. 3. Definition of stress orientation angle (see also Fig. 5)

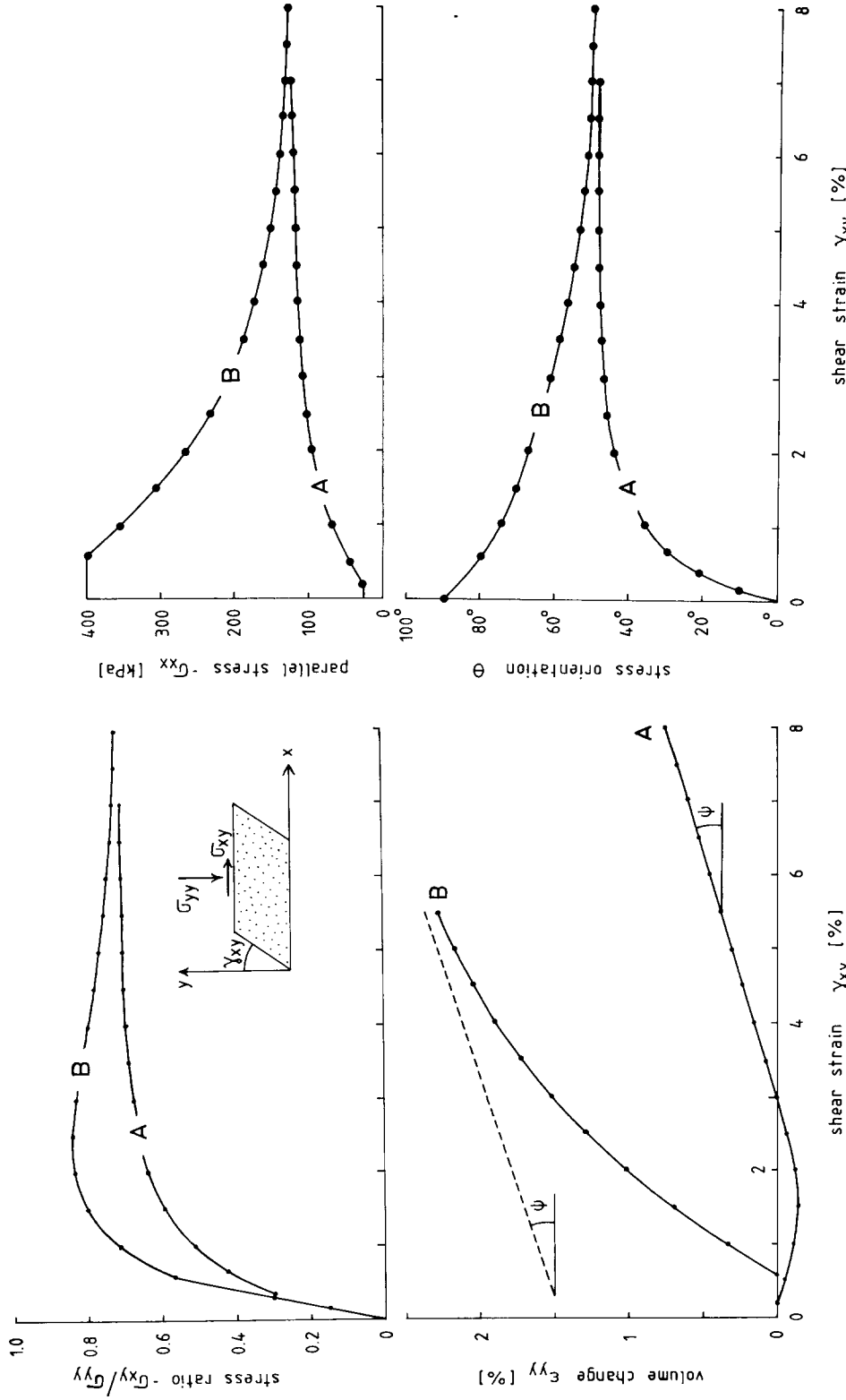

Fig. 4. Numerical results for simple shear tests: (a, b) conventional stress–strain plots; (c) evolution of horizontal stress; (d) stress rotation

the stress circle touches Coulomb's envelope, and the sample yields plastically. The non-linear elastoplastic response is computed from Equation (10), or written in full

$$\left.\begin{aligned}\dot{\sigma}_{xx} &= M_{11}\dot{\varepsilon}_{xx} + M_{12}\dot{\varepsilon}_{yy} + M_{13}\dot{\gamma}_{xy}\\ \dot{\sigma}_{yy} &= M_{21}\dot{\varepsilon}_{xx} + M_{22}\dot{\varepsilon}_{yy} + M_{23}\dot{\gamma}_{xy} = 0\\ \dot{\sigma}_{xy} &= M_{31}\dot{\varepsilon}_{xx} + M_{32}\dot{\varepsilon}_{yy} + M_{33}\dot{\gamma}_{xy}\end{aligned}\right\} \quad (16)$$

The condition $\dot{\sigma}_{yy} = 0$ is due to the fact that the vertical stress is kept constant during the test. Simple shear testing also involves zero horizontal strain so that the additional condition $\dot{\varepsilon}_{xx} = 0$ is obtained. Hence the second one of Equations (16) can be solved to obtain

$$\dot{\varepsilon}_{yy} = -(M_{23}/M_{22})\dot{\gamma}_{xy}$$

Using this expression, and again $\dot{\varepsilon}_{xx} = 0$, it is found from Equation (16) that

$$\dot{\sigma}_{xx} = M_{22}^{-1}(-M_{12}M_{23} + M_{13}M_{22})\dot{\gamma}_{xy} \quad (18a)$$

$$\dot{\sigma}_{xy} = M_{22}^{-1}(-M_{32}M_{23} + M_{33}M_{22})\dot{\gamma}_{xy} \quad (18b)$$

or using Equations (10), (13) and (14):

$$\dot{\sigma}_{xx} = -2G^* \sin 2\theta(\cos 2\theta + \sin\psi)\dot{\gamma}_{xy} \quad (19a)$$

$$\dot{\sigma}_{xy} = G^*(\cos 2\theta + \sin\psi)(\cos 2\theta + \sin\phi)\dot{\gamma}_{xy} \quad (19b)$$

with

$$G^* = G\{2\sin^2 2\theta + (\cos 2\theta + \sin\psi) \times (\cos 2\theta + \sin\phi)\}^{-1}$$

The above differential equations for the stress rates can be integrated numerically to obtain Fig. 4. Here Euler's forward marching technique was applied, updating θ at the beginning of each increment by using Equation (15).

Results for normally consolidated sample

With the normally consolidated sample, both the shear stress (Fig. 4(a)) and parallel stress, σ_{xx} (Fig. 4(c)), increase monotonically with the shear strain. Fig. 4(d) shows the orientation of the minor compressive stress against the horizontal. This stress orientation angle starts off at zero and increases to become equal to $\theta_R = 45° + \frac{1}{2}\psi$. This particular value also follows from Equations (19) and the requirement that all stresses finally become stationary. Indeed, it follows from the steady-state conditions $\dot{\sigma}_{xx} = \dot{\sigma}_{xy} = 0$, that $(\cos 2\theta + \sin\psi) = 0$ which gives the ultimate value of $\theta = \theta_R$.

sample A: $0 \leqslant \theta \leqslant \theta_R = 45° + \frac{1}{2}\psi$

Results for overconsolidated sample

In this case of an overconsolidated sample the vertical stress is the minor compressive stress so that there is an initial θ value of 90°. The striking difference with the A-test is the softening behaviour that is shown in Fig. 4(a), but this is to be commented on later. Another phenomenon is the considerable increase of volume as seen in Fig. 4(b). Fig. 4(c) shows that the initially large parallel stress decreases to reach the same steady-state value as for the normally consolidated sample. As a consequence, the stress orientation angle also decrease, from $\theta = 90°$ down to $\theta = \theta_R$.

sample B: $90° \geqslant \theta \geqslant \theta_R = 45° + \frac{1}{2}\psi$

For this particular range of θ values, the shear–stress curve of Fig. 4(a) shows a marked peak and then a softening down to the residual strength. Both at peak and at the residual strength there is $\dot{\sigma}_{xy} = 0$. If this condition is inserted in Equation (19(b)) it follows that

$$(\cos 2\theta + \sin\psi)(\cos 2\theta + \sin\phi) = 0 \quad (21)$$

which gives the solutions $\theta = \theta_R$ and $\theta = \theta_C$. The first value corresponds to the peak strength in Fig. 4(a) and the second value gives the residual strength. These particular values for θ can now be used to calculate stress ratio σ_{xy}/σ_{yy} at peak and residual strength respectively. To this end a general equation for the stress ratio can first be derived. On using the yield condition $f = 0$ in combination with Equations (11) and (15) it follows that

$$\frac{\sigma_{xy}}{-\sigma_{yy}} = \frac{\sin 2\theta \sin\phi}{1 + \cos 2\theta \sin\phi} \quad (22a)$$

This applies to a non-cohesive material. Inserting the special values of θ_C and θ_R, it is found that

$$\left(\frac{\sigma_{xy}}{-\sigma_{yy}}\right)_{peak} = \tan\phi \quad (22b)$$

$$\left(\frac{\sigma_{xy}}{-\sigma_{yy}}\right)_{residual} = \tan\alpha$$

$$\tan\alpha \equiv \frac{\cos\psi \sin\phi}{1 - \sin\psi \sin\phi} \quad (22c)$$

The peak stress ratio for $\theta = \theta_C$ appears to involve the well-known factor $\tan\phi$, but the residual stress ratio involves a lower factor. In the special case of a non-dilating soil ($\psi = 0$), the above residual ratio simply reduces to $\sin\phi$. On the other hand, for an associated flow rule with $\psi = \phi$, the residual ratio would also be $\tan\phi$ as for the peak ratio. In reality, however, the dilatancy angle is not equal to the friction angle, but significantly smaller. For quartz sand there is the empirical rule $\psi \simeq \phi - 30°$ as used in Table 1.

Table 1. Apparent friction angle α as computed for simple shear

ϕ: deg	ψ: deg	Tan α	α: deg
30	0	0·50	26·56
35	5	0·60	31·03
40	10	0·71	35·47
45	15	0·82	39·29

From this Table it can be observed that the apparent residual friction angle α, deviates about 10% from the real friction ϕ.

Softening

For dense sand, the phenomenon of softening is well known. At yield a dense sand dilates significantly and the plastic dilation creates a looser sand which involves a reduction of the friction angle. Such material degradation does occur in reality, but this is not incorporated in the model. The present model involves a constant friction angle and thus no material degradation at all.

All softening beyond the peak of curve B in Fig. 4(a) comes from the decrease of the horizontal stress σ_{xx}, inside the sample. It is a type of non-associated softening most soil engineers will not be aware of. Here the term non-associated softening is introduced as it occurs only for non-associated flow rules ($g \neq f$).

ONSET OF SHEAR BANDING

As in previous sections, a soil test involving plane strain is considered. This time, however, it is a biaxial test and not a simple shear test. Consider a homogeneous sample, which is loaded up to failure so that the friction angle is fully mobilized. Further deformation is assumed to be localized in a shear band as indicated in Fig.5. For convenience, the x-axis is taken in the yet unknown direction of the shear band. This choice of co-ordinates facilitates a straightforward formulation of the shear band conditions, and a computation of the yet unknown direction of the band.

A shear band is defined as a thin material layer that is undergoing simple shear. The shear band is bounded by two interfaces, on which the rates of stress and strain may be discontinuous to some extent. To formulate the discontinuity conditions, the following notations are adopted—inside the band: $\boldsymbol{\sigma}$ and $\boldsymbol{\varepsilon}$; outside the band: $\boldsymbol{\sigma}^\circ$ and $\boldsymbol{\varepsilon}^\circ$.

Hence a special superscript is introduced to distinguish the exterior stresses and strains from the interior shear-band quantities. At the onset of shear-banding the interior stresses coincide with the exterior ones, but this may change during the actual development of the band.

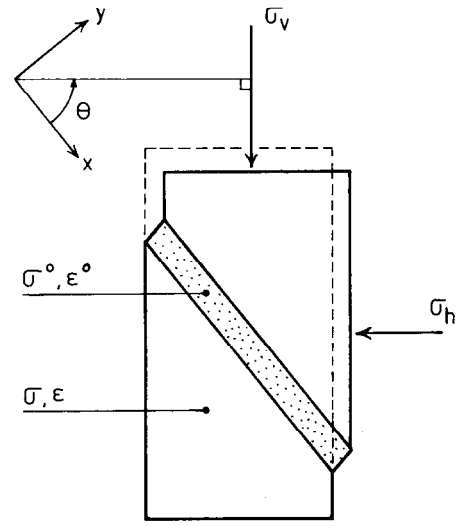

Fig. 5. x-axis is taken in yet-unknown direction of the shear band

For kinematical compatibility it is required that the parallel strain rate $\dot{\varepsilon}_{xx}$ (which is in the direction of the band) corresponds to the corresponding strain rate component outside the band.

$$\dot{\varepsilon}_{xx} = \dot{\varepsilon}_{xx}^\circ \tag{23a}$$

In contrast to the parallel strain, the parallel stress σ_{xx} can become discontinuous across an interface. Here, the stress components which act perpendicularly and tangentially to the interface must be the same on both sides of the interfaces. These static equilibrium conditions read

$$\dot{\sigma}_{yy} = \dot{\sigma}_{yy}^\circ \quad \dot{\sigma}_{xy} = \dot{\sigma}_{xy}^\circ \tag{23b}$$

Consider a biaxial test which is similar to a conventional triaxial test, in the sense that the horizontal cell pressure is kept constant. Let the vertical pressure be increased up to failure so that the sample is in plastic state. Peak strength is reached and on shear-banding the vertical pressure may either remain constant or decrease. Pressure is considered to be negative, so that shear-banding is subject to the additional conditions

$$\dot{\sigma}_v \geqslant 0 \quad \dot{\sigma}_h = 0$$

where the subscript h is used to indicate the horizontal cell pressure, and the subscript v is used for the vertical stress on top of the sample.

Outside the band

The condition on σ_v allows for a possible reduction of the vertical pressure and consequent-

ly an elastic unloading of the material outside the shear band. For the main body of the sample, elastic behaviour is obtained, with

$$\left.\begin{aligned}\dot{\varepsilon}_{xx}^{\circ} &= \dot{\sigma}_{xx}^{\circ}/2G\\ \dot{\varepsilon}_{yy}^{\circ} &= \dot{\sigma}_{yy}^{\circ}/2G\\ \dot{\gamma}_{xy}^{\circ} &= \dot{\sigma}_{xy}^{\circ}/G\end{aligned}\right\} \tag{25}$$

$2G = E$, where E is the Young's modulus, at least for $\nu = 0$ as assumed in this study for the sake of convenience. All these stress rates relate to a possible change of the vertical stress σ_v on top of the sample. Using Mohr's circle and the condition $\dot{\sigma}_h = 0$, it can be shown that

$$\left.\begin{aligned}\dot{\sigma}_{xx}^{\circ} &= \tfrac{1}{2}(1 - \cos 2\theta)\dot{\sigma}_v\\ \dot{\sigma}_{yy}^{\circ} &= \tfrac{1}{2}(1 + \cos 2\theta)\dot{\sigma}_v\\ \dot{\sigma}_{xy}^{\circ} &= -\tfrac{1}{2}\sin 2\theta\dot{\sigma}_v\end{aligned}\right\} \tag{26}$$

Inside the band

The thin layer of material inside the band must be yielding plastically, as elastic strains alone would not show large rates of shearing. This behaviour is therefore governed by the elastoplastic law (10). The latter is a matrix equation which assembles three ordinary equations including

$$\left.\begin{aligned}\dot{\sigma}_{yy} &= M_{21}\dot{\varepsilon}_{xx} + M_{22}\dot{\varepsilon}_{yy} + M_{23}\dot{\gamma}_{xy}\\ \dot{\sigma}_{xy} &= M_{31}\dot{\varepsilon}_{xx} + M_{32}\dot{\varepsilon}_{yy} + M_{33}\dot{\gamma}_{xy}\end{aligned}\right\} \tag{27}$$

By the use of the conditions (23(a), and (b)) and substitution of the expressions (25, 26), Equations (27) become

$$\left.\begin{aligned}\alpha\dot{\sigma}_v &= M_{22}\dot{\varepsilon}_{yy} + M_{23}\dot{\gamma}_{xy}\\ \beta\dot{\sigma}_v &= M_{32}\dot{\varepsilon}_{yy} + M_{33}\dot{\gamma}_{xy}\end{aligned}\right\} \tag{28}$$

where

$$\left.\begin{aligned}2\alpha &= 1 + \cos 2\theta - (1 - \cos 2\theta)M_{21}/2G\\ 2\beta &= -\sin 2\theta - (1 - \cos 2\theta)M_{31}/2G\end{aligned}\right\} \tag{29}$$

Now the normal strain rate $\dot{\varepsilon}_{yy}$ can be eliminated easily from Equations (28) to obtain

$$\dot{\sigma}_v = \frac{M_{33}M_{22} - M_{32}M_{23}}{\beta M_{22} - \alpha M_{32}}\,\dot{\gamma}_{xy} \tag{30}$$

This expression for $\dot{\sigma}_v$ resembles the expression (18(b)) for the rate of shear stress in a conventional simple shear test; only the denominator is different. To get more insight, expressions (10), (13), and (14) are substituted for M_{ij} to find the proportionality

$$\dot{\sigma}_v \propto G(\cos 2\theta + \sin\psi)(\cos 2\theta + \sin\phi)\dot{\gamma}_{xy} \tag{31}$$

as previously obtained for the shear stress in a simple shear test. Again there are two θ values for which the rate of stress vanishes, namely

$$\cos 2\theta + \sin\psi = 0 \quad \text{for } \theta = \theta_R \tag{32a}$$

$$\cos 2\theta + \sin\phi = 0 \quad \text{for } \theta = \theta_C \tag{32b}$$

Hence both the Roscoe-type shear band solution and the Coulomb-type shear band come out as special cases. At the onset of their formation there is no change of the vertical stress. Only impending shear band formation is considered in this section. Later it will be shown that a Coulomb-type shear band will eventually lead to softening (i.e. a reduction of the vertical stress).

ADMISSIBLE SHEAR BAND ORIENTATIONS

From the previous analysis the Roscoe shear band and the Coulomb shear band come out as special solutions but not as the only solutions. To assess other solutions, it is of interest to consider the sign of the vertical stress rate. On inspecting Equation (31) for $\dot{\sigma}_v$, it can be shown from the nominator and the denominator respectively that

$$\theta_R < \theta < \theta_C\colon\ M_{33}M_{22} - M_{32}M_{23} < 0$$

$$0 < \theta < 90^{\circ}\colon\ \beta M_{22} - \alpha M_{33} < 0 \tag{33}$$

Sign $\dot{\sigma}_v$ corresponds to sign $\dot{\gamma}_{xy}$ as long as the shear band is inclined between the Roscoe solution and the Coulomb solution. This implies a decrease in terms of pressure and thus immediate softening at the onset of shear banding. For shear band orientations outside the Roscoe–Coulomb range the vertical pressure would increase, whereas elastic unloading was assumed for the material outside the band. Hence all shear band inclinations within the Roscoe–Coulomb range are possible; other directions are impossible. With the exception of the Roscoe band and the Coulomb band, there is immediate softening. It can easily be derived from Equation (31) that the initial rate of softening is extreme for the intermediate angle $\theta = \theta_A \equiv 45^{\circ} + (\phi + \psi)/4$.

Stress discontinuity

Another interesting phenomenon relates to the parallel stress σ_{xx} inside the shear band. The rate of this normal stress rate can be computed most directly from the condition that the stresses must remain on the yield surface during plastic yielding. This so-called consistency condition reads

$$\dot{f} = \frac{\partial f}{\partial \sigma_{xx}}\,\dot{\sigma}_{xx} + \frac{\partial f}{\partial \sigma_{yy}}\,\dot{\sigma}_{yy} + \frac{\partial f}{\partial \sigma_{xy}}\,\dot{\sigma}_{xy} = 0 \tag{34}$$

Substituting Equation (27) for $\dot{\sigma}_{yy}$ and $\dot{\sigma}_{xy}$, it is found that

$$\dot{\sigma}_{xx} = \frac{1}{2}\left[\sin 2\theta \frac{\partial f}{\partial \sigma_{xy}} - (1 + \cos 2\theta)\frac{\partial f}{\partial \sigma_{yy}}\right]\dot{\sigma}_v \Big/ \frac{\partial f}{\partial \sigma_{xx}} \qquad (35)$$

$$\dot{\sigma}_{xx}^{\circ} = \frac{1}{2}(1 - \cos 2\theta)\dot{\sigma}_v \qquad (26^*)$$

The above expression for the stress rate outside the band is simply a repetition of Equation (26). Because of the difference from the stress rate $\dot{\sigma}_{xx}$ inside the band, there is a stress discontinuity across the interfaces. Using the above expressions and elaborating the first one in more detail, it can be shown that

$$\delta\dot{\sigma}_{xx} = \dot{\sigma}_{xx} - \dot{\sigma}_{xx}^{\circ} = \frac{1 - \sin\phi}{\cos 2\theta + \sin\phi}\dot{\sigma}_v \qquad (36)$$

or by substituting Equation (31)

$$\delta\dot{\sigma}_{xx} \propto (\cos 2\theta + \sin\psi)\dot{\gamma}_{xy}$$

This equation implies that generally a stress discontinuity will develop across the boundaries of a shear band. It is only for a Roscoe-type shear band with $\cos 2\theta + \sin\psi = 0$ that there is no change of the parallel stress. Actually, the Roscoe-type band is a special case as all stress components remain stationary, including σ_{yy} and σ_{xy}. The change of parallel stress becomes extreme for the Coulomb-type shear band. Findings may now be summarized

$\theta = \theta_R$: all stress rates vanish, no softening at all

$\theta = \theta_A$: extreme rate of initial softening

$\theta = \theta_C$: extreme change of parallel stress

All three solutions which are frequently observed in practice therefore come out as special cases.

POST-BIFURCATION ANALYSIS

Having considered the onset of shear banding, the stress–strain behaviour beyond the bifurcation point will now be studied. For a Roscoe-type shear band this is trivial as stresses remain stationary, both outside and inside the shear band. For other shear bands, however, stresses do change and this effect will be quantified for a cohesionless less sand with the properties

$$G = 10\,\text{MPa} \quad \phi = 40^\circ \quad \psi = 10^\circ$$

In contrast to the bifurcation analysis for the onset of shear banding, a numerical analysis has now to be performed. The procedure of such a numerical computation will be outlined in this section. Numerical results will be given for a biaxial sample that has been loaded up to failure with

$$\sigma_h = -100\,\text{kPa} \quad \sigma_v = \frac{1 + \sin\phi}{1 - \sin\phi}\sigma_h$$

Up to this state of stress the sample has deformed homogeneously. Hereafter a shear band develops, say an intermediate one with $\theta = \theta_A$. As in previous sections, the x-axis of the Cartesian coordinates is taken in the direction of the shear band as indicated in Figs 5 and 6.

The first step of the numerical analysis is the computation of the Cartesian stress components from the principal stresses σ_h and σ_v. Mohr's stress circle can now be used to derive that

$$\sigma_{xx} = \tfrac{1}{2}(\sigma_h + \sigma_v) + \tfrac{1}{2}(\sigma_h - \sigma_v)\cos 2\theta_A \qquad (38a)$$

$$\sigma_{yy} = \tfrac{1}{2}(\sigma_h + \sigma_v) - \tfrac{1}{2}(\sigma_h - \sigma_v)\cos 2\theta_A \qquad (38b)$$

$$\sigma_{xy} = \tfrac{1}{2}(\sigma_h - \sigma_v)\sin 2\theta_A \qquad (38c)$$

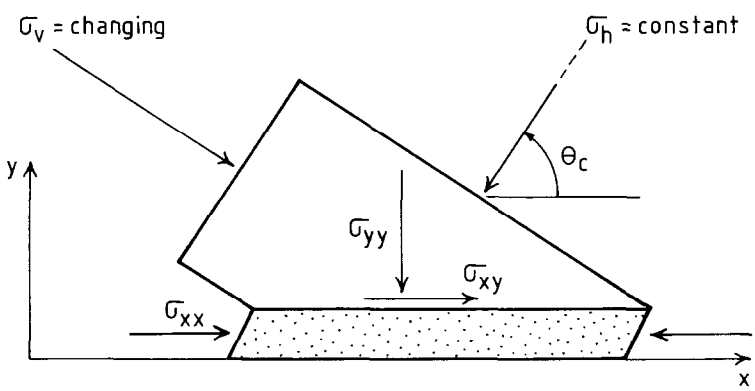

Fig. 6. Shear-banding resembles simple shear testing to some extent

At the onset of shear banding this state of stress is applied to the entire sample (i.e. $\boldsymbol{\sigma} = \boldsymbol{\sigma}^{\circ}$). Hereafter the inside-parallel stress σ_{xx} will begin to deviate from the outside-parallel stress σ_{xx}°.

The second step of the numerical analysis is the computation of the increment of the vertical stress σ_v for a given increment of the shear strain γ_{xy} inside the shear band. Let $\Delta\sigma_v$ denote a small increment of vertical stress and let $\Delta\gamma_{xy}$ be a small increment of shear strain, then it follows from Equation (30) that

$$\Delta\sigma_v \simeq \frac{G^2(\cos 2\theta + \sin\psi)}{(1 + \sin\phi \sin\psi)} \frac{(\cos 2\theta + \sin\phi)}{(\beta M_{22} + \alpha M_{32})} \Delta\gamma_{xy} \qquad (31^*)$$

$$\sigma_v := \sigma_v + \Delta\sigma_v$$

Here the elastoplastic stiffness M_{ij} are computed from Equations (10) and (13). Conforming with Equation (29) the parameters α and β are computed from

$$2\alpha = 1 + \cos 2\theta - (1 - \cos 2\theta_A) M_{21}/2G$$

$$2\beta = -\sin 2\theta_A - (1 - \cos 2\theta_A) M_{31}/2G \qquad (29^*)$$

The third step in the numerical analysis is the computation of the new Cartesian stress components. For the material outside the shear band this is readily done from Equations (38), using the updated value for the vertical stress. As the stress components σ_{yy} and σ_{xy} have no discontinuity, one is left with the computation of σ_{xx} inside the shear band.

Several options exist for evaluating the new parallel stress, but it is most directly computed from the yield condition $f = 0$ as specified by Equations (11) and (12). This quadratic equation can be solved for σ_{xx} either exactly or approximately by linearization. Another way of calculating the parallel stress is to use the constitutive matrix Equation (10). Here the increments $\Delta\gamma_{xy}$, $\Delta\sigma_{yy}$ and $\Delta\sigma_{xy}$ are known, so that all other three increments $\Delta\sigma_{xx}$, $\Delta\varepsilon_{yy}$ and $\Delta\varepsilon_{xx}$ can be computed.

Having determined all three stress components, the stress direction angle is updated from the well-known equation

$$\theta = \frac{1}{2} \tan^{-1} \frac{2\sigma_{xy}}{\sigma_{xx} - \sigma_{yy}} \qquad (15^*)$$

which conforms with Equation (15). This angle acts inside the shear band—outside the band the stress direction angle remains θ_A.

Steps two and three of the above computations can easily be repeated to obtain a numerical integration procedure. For each computation loop, the vertical stress increment is computed from a given increment of shear strain, and used to compute the other stress increments. The resulting stress–strain curves are shown in Fig. 7. With the exception of the Roscoe solution, all shear bands show softening. Such bands are comparable with simple shearing of overconsolidated samples as shown previously by curve B in Fig. 4(a). The softening is even more pronounced than the softening in simple shear tests. The difference with the simple shear test is the decrease of the stress σ_{yy}, which acts normal to the shear band. A drop of this normal stress will obviously enhance the softening. Fig. 8 shows computational results for the stress orientation angle inside the shear band.

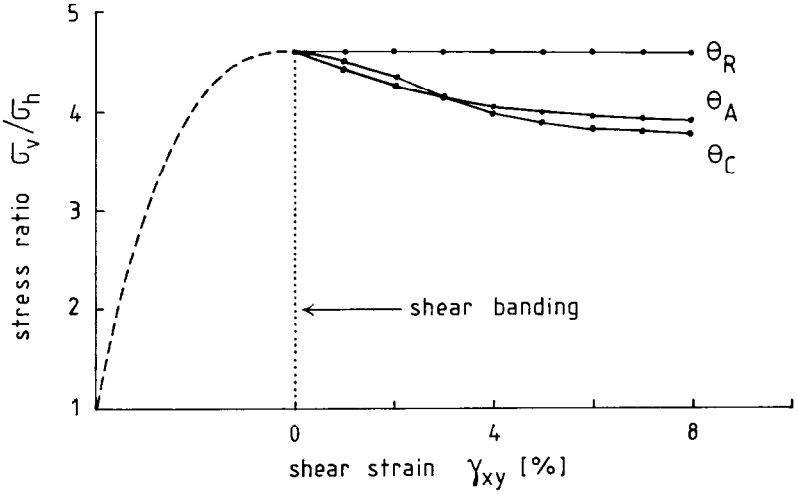

Fig. 7. Computed softening during shear-banding; γ_{xy} is shear strain inside band

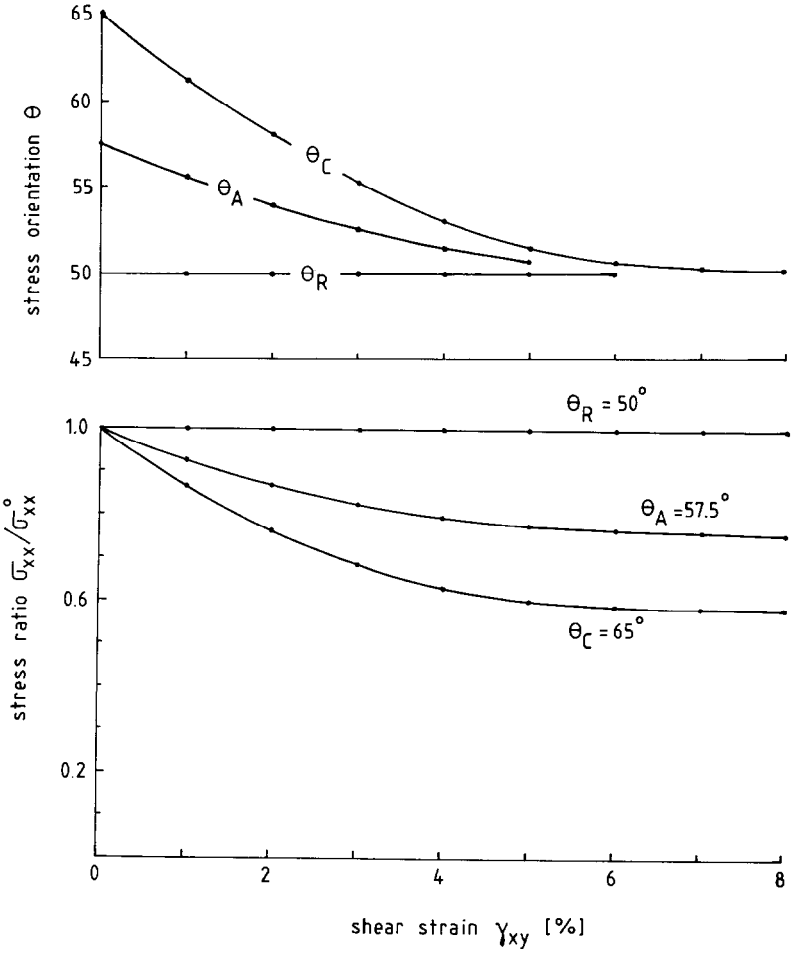

Fig. 8. Further results of post-bifurcation analysis: (a) stress rotation inside shear band; (b) evolution of stress discontinuities

CRITICAL ORIENTATION

As in the simple shear test, it is possible to assess the final residual state of a biaxial test by analytical derivations. Shear banding corresponds to simple shearing so that formulas can be used as derived for the residual strength of a simple shear sample. According to Equation (22c)

$$\left(\frac{\sigma_{xy}}{-\sigma_{yy}}\right)_{\text{residual}} = \tan\alpha$$

$$\tan\alpha \equiv \frac{\cos\psi \sin\phi}{1 - \sin\psi \sin\phi} \qquad (22c^*)$$

The value of α is usually close to the friction angle; Table 1 indicates values slightly below the value of ϕ. Equation (22c) applies to all shear bands independent of the shear band orientation. It can be used to obtain an expression for the residual vertical stress. To this end Equations (38b) and (38c) are inserted which yields

$$\left(\frac{\sigma_v}{\sigma_h}\right)_{\text{residual}} = \frac{\sin(2\theta - \alpha) + \sin\alpha}{\sin(2\theta - \alpha) - \sin\alpha} \qquad (39)$$

where θ is the orientation of the shear band. Using Equation (38) for σ_{yy} and σ_{xy}, θ_A has been replaced by θ as to introduce a particular shear band orientation into the formula would be undesirable. The question of which shear band is most likely to occur in soil testing is to be addressed in the following.

In the derivation of the most critical shear band inclination, it is postulated that collapsing soil bodies will reach the lowest residual load under continuing deformation. This means that

Table 2. Peak and residual stress ratios for critical shear band

Angles: deg			$\frac{\sigma_v}{\sigma_h}$ peak	$\frac{\sigma_v}{\sigma_h}$ residual	$\frac{\sigma_{xx}}{\sigma_{xx}^{\circ}}$ residual
ϕ: deg	ψ: deg	α: deg			
30	0	26·6	3·0	2·6	0·63
35	5	31·0	3·7	3·1	0·60
40	10	35·0	4·6	3·7	0·57
45	15	39·3	5·8	4·6	0·54

the ultimate failure mechanism corresponds to the weakest mechanism. In order to obtain the most critical shear band, the expression for the stress ratio must be minimized with respect to shear band orientation θ. Such a minimum is obtained for

$$\frac{d(\sigma_v/\sigma_h)}{d\theta} = \frac{-4 \sin \alpha \cos (2\theta - \alpha)}{[\sin (2\theta - \alpha) - \sin \alpha]^2} = 0 \qquad (40)$$

which yields the shear band orientation

$$\theta = 45^\circ + \tfrac{1}{2}\alpha \simeq 45^\circ + \tfrac{1}{2}\phi \qquad (41)$$

The angle α is usually only 4 or 6° smaller than the friction angle, so the critical shear band orientation is almost equal to the Coulomb orientation. The error on the shear band orientation is less than 5% when ϕ is used instead of α. In contrast, precise values for α are needed when evaluating the formula

$$\left(\frac{\sigma_v}{\sigma_h}\right)_{residual} = \frac{1 + \sin \alpha}{1 - \sin \alpha} \qquad (42)$$

as obtained by substitution of $\theta = 45^\circ + \alpha/2$ into Equation (39). The residual stress ratio is very sensitive in α as can be seen from Table 2, where the peak stress ratio is computed by the use of ϕ instead of α in Equation (42).

In terms of stress ratios the amount of softening is considerable. For instance, a loose non-dilating sand with a friction angle of 30° shows a peak stress ratio of 3·0 and a residual stress ratio of 2·6. For a dense dilating sand with a friction angle of 45°, the softening becomes extreme as the stress ratio drops from 5·8 to 4·6 (i.e. 20%). In reality a dense sand will soften even more than 20% of its peak strength. A dense sand becomes looser because of plastic dilation so that the friction angle will not remain constant as assumed in this Paper.

STRESS DISCONTINUITIES

Having considered the drop of the stress ratio, it is of interest to consider the change of the parallel stress inside the shear band. For the ratio of the two normal stresses inside the shear band the stress orientation angle $45^\circ + \psi/2$ and Mohr's stress circle can be used to show that

$$\left(\frac{\sigma_{xx}}{\sigma_{yy}}\right)_{residual}^{inside} = \frac{1 + \sin \psi \sin \phi}{1 - \sin \psi \sin \phi} \qquad (43)$$

Outside the shear band there is a different stress ratio as here the stress orientation angle corresponds to the critical shear band inclination $45^\circ + \alpha/2$, so that

$$\left(\frac{\sigma_{xx}}{\sigma_{yy}}\right)_{residual}^{outside} = \frac{1 + \sin \alpha \sin \phi}{1 - \sin \alpha \sin \phi} \qquad (44)$$

Equations (43) and (44) can now be combined to obtain for the parallel stresses inside and outside the shear band

$$\frac{\sigma_{xx}^{inside}}{\sigma_{xx}^{outside}} = \frac{1 + \sin \psi \sin \phi}{1 - \sin \psi \sin \phi} \times \frac{1 - \sin \alpha \sin \phi}{1 + \sin \alpha \sin \phi} \qquad (45)$$

Particular values for this stress ratio are listed in Table 2 and appear to be of the order of 0·6. Ratios of 0·6 indicate a considerable stress discontinuity across the boundary lines of shear bands. This creates effects at the beginning and the end of a shear band (i.e. at the boundaries of the sample, which have not been considered in previous sections). If uniform boundary tractions and internal stresses are assumed, there would be an out-of-balance force at the shear band endings. It follows for the out-of-balance force that

$$F = (\sigma_{xx}^{out} - \sigma_{xx}^{in}) d_b \quad d_b \simeq 15 d_{50} \qquad (46)$$

where d_b is the thickness of the band and d_{50} is the mean particle size. Hence coarse sands create a larger out-of-balance force than fine sands. Compare, for instance, a fine sand with a mean particle size of 0·2 mm and a coarse sand with a mean particle size of 1·4 mm. A shear band in the fine sand will have a thickness of only 3 mm, but the coarse sand will lead to 21 mm. For a relatively thin shear band in fine sand, the low out-of-balance forces can easily be accommodated by the rubber membrane that surrounds the sample.

The thickness of the membrane is usually about 0·4 mm, and consequently thicker than the particle diameter of fine sand. Such a membrane can easily accommodate some suction at the tips of the shear band.

For coarse sand, the significant thickness and relatively large out-of-balance force give end-effects which cannot easily be equilibrated by the rubber mould around the sample. As a consequence shear bands with stress discontinuities are not likely to develop. Instead, Roscoe-type shear bands are likely to occur, as also observed in experiments (see the second section). It is the ratio of shear band thickness to rubber membrane thickness rather than simply the particle size which decides on the occurrence of a particular type of shear band.

CONCLUSIONS

Experimental data as reviewed in this Paper indicate that the orientation of shear bands varies between the limits of $\theta_R = 45° + \psi/2$ and $\theta_C = 45° + \phi/2$, depending on the particle size of the sand considered. The experimental evidences show that coarse sands tend to give the Roscoe-orientation θ_R, whereas fine sands tend to give the Coulomb-orientation θ_C. A theoretical analysis for the onset of shear-banding, as presented in this study also yields the above solutions as limits for possible shear-band orientations. What is new in this analysis is the allowance of elastic unloading and the finding that there are not one or two possible orientations at a given state of stress, but a wide range of admissible orientations.

Another item of this Paper is the post-bifurcation analysis for situations well beyond incipient shear banding. This extension of the analysis is needed in order to determine the type of shear band which is most likely to occur. For convenience, material degradation due to material dilation is not modelled. Having not modelled such intrinsic material weakening, one would not expect to obtain a softening response when simulating shear-banding in biaxial samples. Nevertheless such a response is obtained. As soil samples will tend to fail corresponding to the weakest failure mode, Coulomb-type shear-banding appears to be the preferred failure mechanism, as generally observed for fine sands. In fact the exact Coulomb orientation was not found but a slightly smaller inclination. On a second inspection of experimental data, this appears to be realistic.

As experimental data for coarse sands do not show the Coulomb orientation but the Roscoe orientation, the stress discontinuities associated with most shear banding have been analysed. The computed changes of the parallel stress inside a Coulomb-type shear band give an explanation for the fact that such shear bands seldom occur in biaxial samples of coarse sand. Coarse sand implies relatively thick shear bands so that a drop of the parallel stress would yield out-of balance forces at the far ends of the shear band that were too large. Instead, Roscoe-type shear bands are likely to occur in biaxial samples of coarse sand.

The consequences of the findings for shear banding in model tests and in situ situations are not yet clear. For large soil bodies the thickness of shear bands is negligible compared with the dimensions of the body, so that the effect of the out-of-balance forces might disappear. In such situations all inclinations between the Roscoe solution and the Coulomb solution seem to be feasible. As in the analysis for the biaxial test, the residual collapse mechanism is expected to be the weakest mechanism. For complex mechanisms and external constraints, this need not lead to just the Coulomb orientation or just the Roscoe orientation, but can also lead to other orientations in between the two extremes. Scarpelli and Wood (1982) report among others complex patterns of shear bands in a medium fine sand which is sheared in a long simple shear apparatus; shear band orientations are found to exist in between the two extremes.

REFERENCES

Arthur, J. R. F., Dunstan, T., Al-Ani, Q. A. J. & Assadi, A. (1977). Plastic deformation and failure of granular media. *Géotechnique* **27**, No. 1, 53–74.

Arthur, J. R. F. & Dunstan, T. (1982). Rupture layers in granular media. *Proc. IUTAM Symp. Deformation and Failure of Granular Materials, Delft* (eds P. A. Vermeer & H. J. Luger), pp. 453–459. Rotterdam: Balkema.

Bransby, P. L. & Milligan, G. W. E. (1975). Soil deformations near cantilever sheet pile walls. *Géotechnique* **25**, No. 2, 175–195.

Desrues, J. (1984). *La localisation de la déformation dans les matériaux granulaires.* PhD dissertation, Institut National Polytechnique de Grenoble, Grenoble, 283 pp.

Desrues, J. & Hammad, W. (1989). Experimental study of the localization of deformation in sand: influence of mean stress. *Euromech, Colloquium 248 on non-linear soil-structure interaction, Grenoble.*

Duthilleul, B. (1982). *Rupture progressive: simulation physique et numérique.* PhD dissertation, Institut National Polytechique de Grenoble, Grenoble, 260 pp.

Mandel, J. (1966). Condition de stabilité et postulat de Drucker. *Proc. Symp. Rheology and Soil Mechanics, Grenoble*, pp. 58–68. Berlin: Springer-Verlag.

Roscoe, K. H. (1970). The influence of strains in soil mechanics. *Géotechnique* **20**, No. 2, 129–170.

Scarpelli, G. & Wood, D. M. (1982). Experimental observations of shear band patterns in direct shear tests. *Proc. IUTAM Symp. Deformation and Failure of Granular Materials, Delft*, (eds P. A. Vermeer & H. J. Luger), pp. 473–484. Rotterdam: Balkema.

Vardoulakis, I. (1980). Shear band inclination and shear modulus of sand in biaxial tests. *Int. J. Numer. and Analyt. Methods in Geomech.* **4,** 103–119.

Vardoulakis, I. (1988). Private communication.

Vermeer, P. A. (1982). A simple shear band analysis using compliances. *Proc IUTAM Symp. Deformation and Failure of Granular Materials, Delft*, (eds P. A. Vermeer & H. J. Luger), pp. 493–499. Rotterdam: Balkema.

Vermeer, P. A. & de Borst, R. (1984). Non-associated plasticity for soil, concrete and rock. *HERON* **29,** No. 3, 1–64.

Wood, D. M. & Budhu, M. (1980). The behaviour of Leighton Buzzard sand in cyclic simple shear tests. *Proc. Int. Symp. Soils under Cyclic and Transient Loading, Swansea*, (eds G. N. Pande and O. C. Zienkiewicz), pp. 9–21. Rotterdam: Balkema.